Optimizing 1D Dielectric Electromagnetic Bandgap (D-EBG) Structures Using Multistage Genetic Algorithm (MS-GA) and Considering Parameter Variations

Chouwei Guo, Yusheng Hu*, Lijin He, and Mengyuan Niu

Abstract—An optimization method utilizing a multistage genetic algorithm (MS-GA) and considering parameter variations has been proposed to obtain optimal design of one-dimensional dielectric bandgap (1D D-EBG) structures with a few periods in small packaging power distribution networks. One-dimensional finite method (1D FEM) is used to improve computational efficiency and iteration speed. MS-GA consists of 3 stages: In stage 1, the population was initialized by Hamming distance, and the fitness was calculated to determine the number of EBG period. In stage 2, genetic manipulation and sensitivity analysis were used to improve local search ability and obtain preliminary results. In stage 3, cubic spline interpolation and local integral were used to reconstruct the fitness evaluation function considering parameter deviation, adjust the results, and obtain the optimal parameters. Three optimized target frequency bands with center frequencies of 2.4 GHz, 3.5 GHz, and 28 GHz were optimized, and Pearson coefficient was used to analyze the correlation between the parameters to better understand the influence of parameter deviation on the optimization results. The achieved results meet the optimization object within the allowable range of parameter errors, and the parameter constraints were successfully met for all three designs, with their final dimensions below 20 mm. Three-dimensional full-wave simulation software was used to simulate and analyze the stopband bands, and the simulation results were consistent with the calculation results.

1. INTRODUCTION

With the improvement of high-speed circuit performance, ground bounce noise and synchronous switch noise (SSN) have become one of the major concerns in high-speed packages and printed circuit board (PCB) design. Power distribution networks (PDNs) have become the main propagation path of electromagnetic noise. Meanwhile, the resonance between power/ground planes can lead to serious signal integrity (SI) issues and power integrity (PI) problems [1]. Thus, various suppression strategies have been proposed, such as segmented power/ground plane [2] and embedded capacitor [3]. However, at higher frequencies, electromagnetic noise can still couple through gaps. The use of electromagnetic band gap (EBG) structures is a promising approach to address high-frequency electromagnetic interference. It is a periodic structure that shows stopband effect in a specific frequency range. High-impedance surface EBG [4], coplanar EBG [5], and dielectric electromagnetic bandgap (D-EBG) structures [6] have been proposed. Among them, D-EBG substrates has the advantages of high reflectivity without breaking the circuit's signal integrity, effectively controlling the electromagnetic wave wavelength in small-sized packages with high integration. Although these wide bandgap structures have been widely used in fields such as microwave bandstop filters, microwave power amplifiers, antennas, and resonant cavities, their

research on noise suppression in power distribution networks, especially in small-sized packaging and intelligent optimization design, requires further investigation.

In order to achieve wider stopband and higher suppression depths in PDN, various types of intelligent algorithms have been applied to the optimization of EBG structures, including cuckoo search algorithm [7], genetic algorithms [8], global evolutionary algorithm [9], and swarm intelligence algorithm [10]. Among them, genetic algorithm is widely used in the field of electromagnetic engineering due to its ease of implementation and strong robustness [11, 12]. In antenna design [13], microwave imaging [14], filter design [16], and power distribution network design [8], genetic algorithms are introduced to optimize the structural parameters. Ref. [15] introduces a multiobjective evolutionary algorithm that is capable of handling unconstrained and constrained, single and multiobjective problems without any restriction on the number and nature of variables, constraints, and objectives. Ref. [8] combines genetic algorithms with multilayer finite difference method and dispersion diagram to obtain co-planar EBG structures that meet design specifications. Ref. [16] proposes a hybrid genetic algorithm combined with the stepladder macro-zone for fast calculation of the dispersion diagram. Ref. [17] proposes an electromagnetic optimization hybrid algorithm based on genetic algorithm and evolutionary strategy, which overcomes the limitation of genetic algorithm easily falling into local optimal solution. In [18], a new fuzzy genetic algorithm (FGA) is developed to optimize the ground plane with dielectric electromagnetic bandgap (D-EBG) structure. Some improved genetic algorithms have been proposed successively to accelerate the convergence speed, improve the result accuracy, and expand the band gap bandwidth [19–21]. Although these optimize strategies have good application in the structural design of EBG structures in multi-layer packaging systems, there are a few designs for EBG in small-size packaging [22–25]. The current algorithms mainly focus on dispersion curve and forbidden band, while the power distribution network electromagnetic interference suppression mainly focuses on noise isolation. It should be noted that forbidden band gap is calculated based on infinite periods, which makes it unable to present the noise isolation degree in limited periods. In addition, Bloch/Floquet boundary conditions are generally used in the current algorithms, which are in good agreement with the infinite periodic structure, but for the less periodic structure EBG, it is difficult to meet the strict Bloch/Floquet boundary conditions, so the calculation error is large. Moreover, the parameter deviation caused by processing is a factor that cannot be ignored, and the dielectric constant of the material is usually discontinuous, unfixed, and susceptible to external factors, so it can be challenging to obtain materials that have a stable dielectric constant for specific applications.

This article proposes a method for 1D D-EBG structure design with a few periods, in which parameter variations are considered, called the multistage genetic algorithm. In this paper, we use 1D FEM to calculate the stopband with a specified isolation, which can improve computational efficiency and iteration speed. The method consists of three stages: In stage 1, a hamming distance initialization population is used to detect the existence of the bandgap by specifying an isolation degree to define the bandgap, thereby avoiding infinite periodic dispersion calculations. In stage 2, sensitivity analysis is applied in each genetic iteration to improve the algorithm's local search ability. In stage 3, the optimization results are adjusted using a new fitness function generated by multidimensional cubic spline interpolation and integral function based on parameter variations, which is the property deviations of high dielectric constant material and tolerance deviation of size design. By using this method, the optimal parameters of 1D D-EBG were determined for various design objective, and the optimization results and their variation patterns were obtained.

2. FINITE ELEMENT METHOD OF 1D D-EBG

Embedding barium titanate ceramics with high dielectric constant into the substrate of Rogers RT/duroid 5880 material ($\varepsilon_r = 2.2$), which has low dielectric constant and low loss, is extensively used in the multilayer PCB of the 5G era.

The established model is a periodic structure formed by alternating distribution of high-dielectric-constant material (Hk) and low-dielectric-constant material (Lk) in a single direction. This periodic structure is embedded in a pair of inner power/ground planes in a multilayer PCB. The noise generated by high-speed signals will be excited at the noise source end and coupled with the signal line at the receiving end. The EBG structure can effectively decouple the noise.
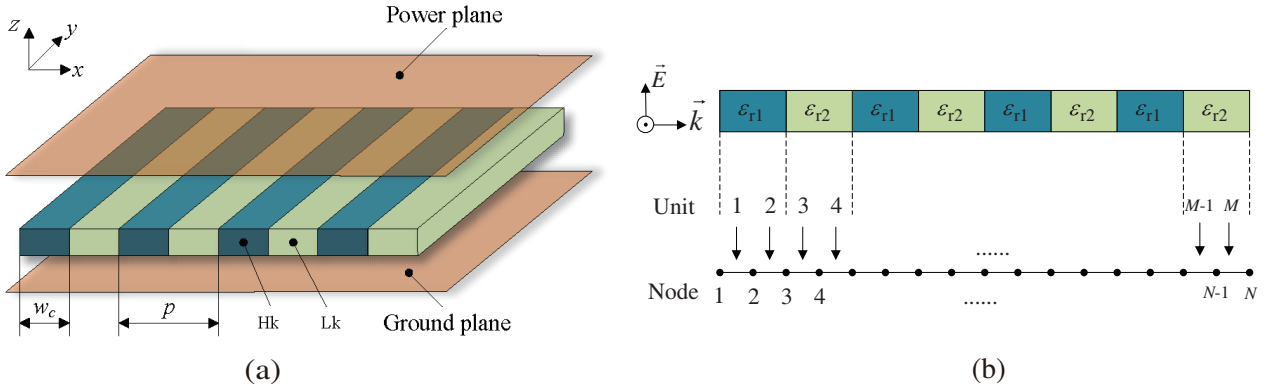
Figure 1. (a) 1D D-EBG power/ground network. (b) Finite element for 1D D-EBG.

The 1D D-EBG structure is shown in Fig. 1(a), with a periodicity of length p, where each EBG unit has HK width w_c, and the dielectric constants of HK and LK are ε_{r1} and ε_{r2}, respectively. In high-speed packaging and multilayer PCB, the dielectric thickness between the power and ground planes is very small, much smaller than the wavelength of the electromagnetic waves being transmitted. So, it is assumed that there is no variation in the electric field along the z-axis. Only the E_z component of the electric field and the H_x and H_y components in the xy plane of the magnetic field exist. Then, the model assumes that the system is infinitely long along the y-axis with uniform and constant dielectric properties, and the gradient of the electric field along the y-axis is zero. Consequently, $H_x = 0$. The final model can be simplified to one-dimension, and only one-dimensional electromagnetic propagation in the x-axis caused by the periodicity of the medium is considered.

The 1D finite element model is shown in Fig. 1(b), where an electromagnetic wave propagates along the x-direction, and the excitation source and receiver are located at the left and right ends, respectively. The model is a line segment of length L containing g D-EBG elements, where the two different dielectric subelements within each EBG element have equal lengths.

The low and high permittivity subelements within each EBG element are discretized into m_1 and m_2 finite element line segments, respectively, resulting in a total of N discrete nodes, $N = (m_1 + m_2)g$. The total number of finite elements in the model is $M = N - 1$, and Fig. 1(b) shows an example with $m_1 = m_2 = 2$. The governing partial differential equation for the electromagnetic field in this model is the one-dimensional Helmholtz equation:

$$\frac{d^2 E_z}{dx^2} + k^2 E_z = 0 \tag{1}$$

where k is the propagation constant, and $k = k_0\sqrt{\varepsilon_r \mu_r}$. k_0 is the wave number in vacuum; ε_r and μ_r are respectively the relative permittivity and relative permeability of the medium. The electric field intensity at the left end of a transmission line can be expressed as

$$E_z = E_z^{\text{inc}} + E_z^{\text{ref}} = E_0 e^{-jk_0 x} + RE_0 e^{jk_0 x} \tag{2}$$

where E_0 represents the amplitude of the given incident wave and can be set to $1\,\text{V/m}$; R represents the reflection coefficient; and E_z^{inc}, E_z^{ref} represent the incident and reflected waves, respectively. Therefore, at the left boundary

$$\frac{dE_z}{dx} = -jk_0 E_0 e^{-jk_0 x} + jk_0 RE_0 e^{jk_0 x} = jk_0 E_z - 2jk_0 E_0 e^{-jk_0 x} \tag{3}$$

Similarly, assuming that the wave at the right end is absorbed by a boundary, it can be expressed as

$$E_z = TE_0 e^{-jk_0 x} \tag{4}$$

where T represents the transmission coefficient. Then, at the right boundary:

$$\frac{dE_z}{dx} = -jk_0 TE_0 e^{-jk_0 x} = -jk_0 E_z \tag{5}$$

The governing differential (1) and boundary conditions (3) and (5) form a boundary value problem. Let $\Phi = E_z$, $\beta = k^2$, then (1) can be expressed as

$$\frac{d^2\Phi}{dx^2} + \beta\Phi = 0 \tag{6}$$

Rewrite (3) and (5) in the form as

$$\frac{d\Phi}{dx} + \gamma\Phi = q \tag{7}$$

It represents the third type of boundary condition, where γ is a parameter related to the physical properties of the boundary, and q is the exciting input at the boundary. For (3), $\gamma_1 = -jk_0$, $q_1 = -2jk_0E_0e^{-jk_0x}$, $x = 0$, and for (5), $\gamma_N = jk_0$, $q_N = 0$, $x = L$.

The equivalent functional of the boundary value problem [26] to be solved is given by

$$F(\Phi) = \frac{1}{2}\int_0^L \left[\frac{d\Phi}{dx}^2 - \beta\Phi^2\right]dx + \left[\frac{\gamma}{2}\Phi^2 - q\Phi\right]_{x=0,L} \tag{8}$$

It contains two terms, the first of which can be written in discrete form

$$F(\Phi) = \sum_{e=1}^{M} F^e(\Phi^e) \tag{9}$$

where e represents the element. $F^e(\Phi^e)$ is the energy functional inside the element defined in

$$F^e(\Phi^e) = \frac{1}{2}\int_{x_1^e}^{x_2^e} \left[\left(\frac{d\Phi^e}{dx}\right)^2 - \beta\left(\Phi^e\right)^2\right]dx \tag{10}$$

where x_1^e and x_2^e are the nodal coordinates of element 'e' with local node numbers 1 and 2. The element stiffness matrix K^e can be obtained by taking the derivative of F^e with respect to Φ_e using the local numbering scheme with nodes as

$$K_{11}^e = K_{22}^e = \frac{1}{l^e} + \beta^e\frac{l_e}{3} \tag{11}$$

$$K_{12}^e = K_{21}^e = \frac{1}{l^e} + \beta^e\frac{l_e}{6} \tag{12}$$

where l^e is the length of the element. After assembling all the element coefficient matrices, the global coefficient matrix K is obtained. The resulting matrix equation is

$$[K]\{\boldsymbol{\Phi}\} = \{\mathbf{b}\} \tag{13}$$

where $\mathbf{b}$ is the zero vector. The second term of the functional in (8) is considered, and let

$$F_b = \left[\frac{\gamma}{2}\Phi^2 - q\Phi\right]_{x=0,L} \tag{14}$$

Due to the boundary condition at node 1, the global coefficient matrix K and vector $\mathbf{b}$ are modified as given in

$$K_{11} = \frac{1}{l^{(1)}} + \beta^{(1)}\frac{l^{(1)}}{3} + \gamma_1 \tag{15}$$

$$b_1 = q_1 \tag{16}$$

Similarly, the global coefficient matrix K for node N is modified as

$$K_{NN} = \frac{1}{l^{(M)}} + \beta^{(M)}\frac{l^{(M)}}{3} + \gamma_N \tag{17}$$

These modifications are made based on the stationary point condition at the boundary nodes

$$K_{NN} = \frac{1}{l^{(M)}} + \beta^{(M)}\frac{l^{(M)}}{3} + \gamma_N \tag{18}$$

Solving the equation group can obtain the total excitation strength at the port of the stimulus source and the absorbing boundary port nodes. Then, the reflection coefficient and transmission coefficient can be calculated. These can be expressed as

$$R = \frac{E_z(x_1) - E_0 e^{-jk_0 x_1}}{E_0 e^{jk_0 x_1}} \tag{19}$$

$$T = \frac{E_z(x_2)}{E_0 e^{-jk_0 x_2}} \tag{20}$$

where $x_1 = 0$ and $x_2 = L$. The scattering parameters expressed in decibels are as

$$S_{11} = 20 \log R \tag{21}$$
$$S_{21} = 20 \log T \tag{22}$$

where S_{11} represents the return loss, and S_{21} represents the insertion loss.

3. MULTISTAGE GENETIC ALGORITHM

3.1. Encoding of 1D D-EBG

Figure 2 represents the design parameter encoding implementation of a 1D D-EBG structure located between the power distribution network and the power ground plane. Here, A, B, and C denote binary-coded individual genotypes, representing the relative dielectric constant (ε_r) of HK, the periodic length (p) of the 1D D-EBG, and the filling ratio (r) of the HK, respectively. The specific sizes of m, n, and k are determined by the precision of the optimized variables. The width w_c of HK in one period can be expressed as

$$w_c = p \cdot r \tag{23}$$

Binary coding is used to generate the initial population P with a population size of N. The individuals in the population of 1D D-EBG structure can be represented by a binary code that concatenates three sets of binary codes representing different genotypes. The binary genotype encoding $[a_1, a_2, a_3, \ldots, a_m]$ corresponds to a decimal number x with the following relationship:

$$x = x_l + (x_h - x_l) \frac{\sum_{j=1}^{m} a_i^j 2^{j-1}}{2^m - 1} \tag{24}$$

where x_l and x_h represent the lower and upper bounds of the optimized parameters in the equation, respectively. The numerical values of the bounds are determined by the machining precision and specific
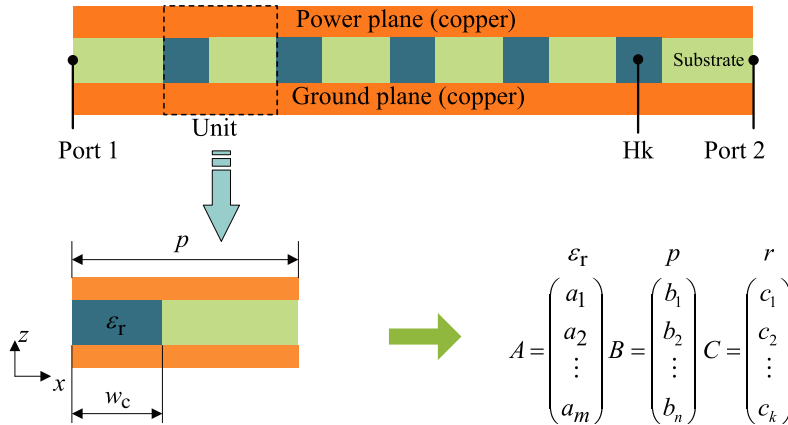

Figure 2. Encoding of 1D D-EBG structure.

design requirements. Individual X is composed of all genotypes including A, B, and C. It can be represented by a one-dimensional matrix as

$$X = [A^T, B^T, C^T] \tag{25}$$

3.2. Multistage Genetic Algorithm

Currently, optimization algorithms mainly focus on optimizing parameters of planar EBG structures. References [7, 9] focused on the automatic design of infinite-period planar EBG structures but did not consider the practical application of finite-period EBGs in noise suppression. Although [8] further considered finite-period noise isolation, the design process was cumbersome, and the size was large. Reference [16] used a hybrid method to calculate the dispersion diagram of metamaterial structures but did not focus on the propagation performance of EBG in finite structures. Additionally, it was applicable to complex 3D modeling and not suitable for 1D electromagnetic characteristic calculations of structures. Reference [18] used a two-dimensional PBG structure as the optimization object and focused on multi-objective optimization of microstrip structure crosstalk, but it was not applicable to wide stopbands and high noise isolation required by PDN applications. Moreover, due to the deviations in dielectric constant, filling ratio, and periodicity length that exist in practical applications, the results obtained from genetic algorithms cannot be implemented accurately. Therefore, this paper proposes a 1D D-EBG structure optimization method combining MS-GA by comprehensively considering the above deficiencies. Fig. 3 shows the design flowchart of MS-GA of this paper.
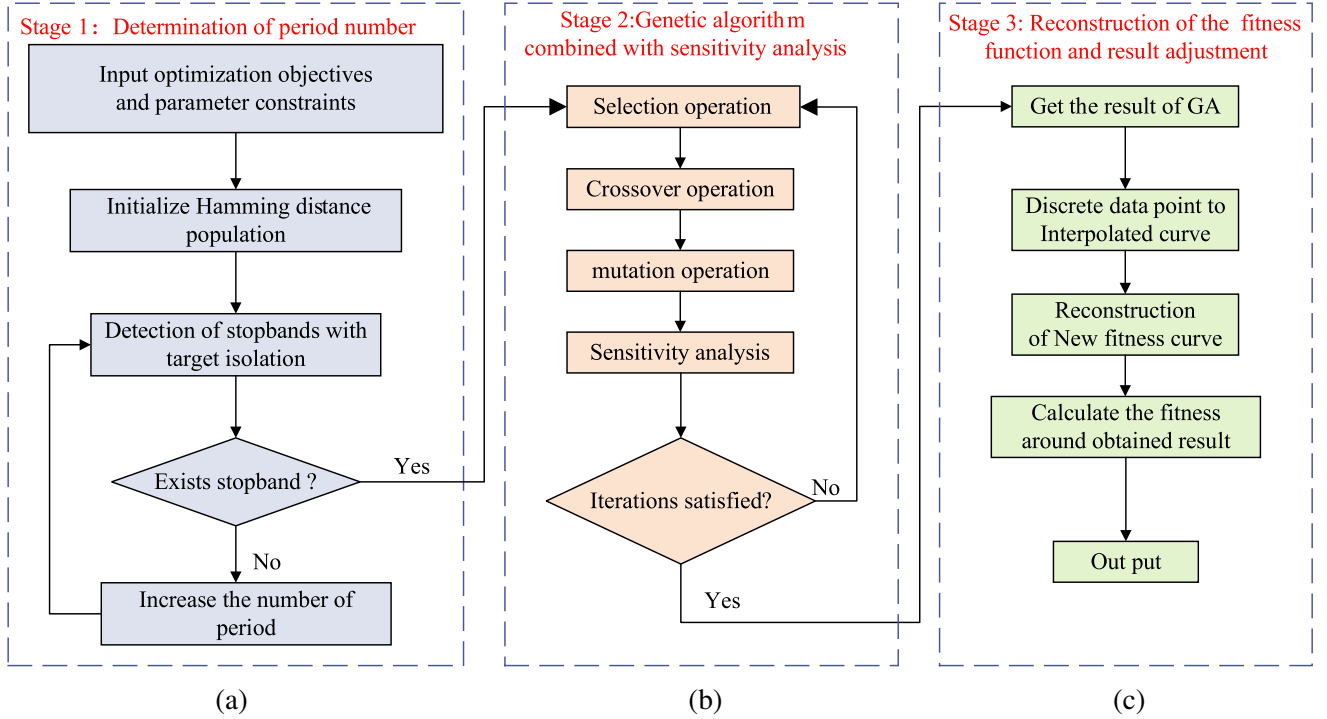

Figure 3. Design flow chart of MS-GA. (a) Stage 1: Determination of period number. (b) Stage 2: Genetic algorithm combined with sensitivity analysis. (c) Stage 3: Reconstruction of the fitness function and result adjustment.

The contributions of this paper can be summarized as follows.

(1) 1D FEM is used to calculate the stopband and isolation of finite-period 1D D-EBG structures without the need for dispersion analysis, with advantages of low computational complexity, high computational efficiency, and easy combination with optimization algorithms. This provides an efficient method for evaluating electromagnetic propagation characteristics of periodic structures while ensuring prediction accuracy.

(2) Combining sensitivity analysis improves the local search ability of the genetic algorithm by utilizing local integration to comprehensively consider the impact of parameter deviations on stopband characteristics, accelerating convergence speed and enhancing design robustness and stability.

(3) Comprehensively considering factors such as stopband width, noise isolation, number of periods, and parameter variation, an automated design scheme for miniaturized, wide stopband, and high noise isolation 1D D-EBG is proposed, making it more beneficial for engineering applications of D-EBG in noise suppression fields.

3.2.1. Stage 1: Determination of Period Number

In basic genetic algorithms, using Hamming distance to initialize a population (Hamming distance population, HD pop) can distribute the population as widely as possible in the solution space to more comprehensively and scientifically characterize the features of the solution space compared to generating populations completely randomly. Hamming distance is the number of positions at which the corresponding symbols in two binary sequences are different. It can be describe as

$$H(x,y) = \sum_{i=1}^{L} [x_i \neq y_i] \tag{26}$$

where x and y represent two binary sequences that are equal-length. L represents the length of sequence. The brackets $[x_i \neq y_i]$ evaluate to 1 if the two symbols are different and 0 if they are same. The sum of all the resulting values gives the Hamming distance between the two strings.

In the initialization stage, the minimum Hamming distance $H_{\min}$ is first set. During the process of generating the initial population randomly, each newly generated individual is compared with every existing individual to determine their Hamming distance. If the Hamming distance between two individuals is less than $H_{\min}$ and greater than 1, it indicates that they are too similar and need to be regenerated. In this article, $H_{\min}$ can be calculated in $H_{\min} = L/2 + 1$.

In the initial stage, it is necessary to first determine the optimization objectives and parameter constraints. The optimization objectives are the target frequency band, B_{set}, and the target isolation degree, S_{set}. The finite element method of 1D D-EBG is applied to obtain the transmission coefficient, S_{21}. The parameter constraints define the range of values for the optimized parameters.

The below criterion for determining the forbidden band isolation:

$$S_{21} \leq S_{\text{set}} \tag{27}$$

The fitness function can be expressed as

$$f(x) = \begin{cases} 0, & B_{\text{set}} \notin B_{\text{gap}} \\ Bw, & B_{\text{set}} \in B_{\text{gap}} \end{cases} \tag{28}$$

where B_{gap} and Bw represent the calculated forbidden band and bandwidth, respectively (in gigahertz). B_{set} is the optimized target frequency range, and it can be expressed as $B_{\text{set}} = (f_l, f_h)$, in which f_l and f_h represent the lower and upper limits of the target frequency band. If the calculated stopband range does not include the target frequency band, the fitness value is 0; otherwise, the fitness value equals the magnitude of the stopband, in gigahertz.

The initialization period is set to 3, and the population is initialized using the minimum Hamming distance. If no individuals in the population have a fitness greater than 0, it can be inferred that there are no parameters that meet the criteria within this period. Subsequently, the period is increased, and the calculation is repeated until a period with a fitness value greater than 0 is found.

3.2.2. Stage 2: Genetic Manipulation Combined with Sensitivity Analysis

The combination of genetic manipulation and sensitivity analysis (SA) has been widely used in biological research. Genetic manipulation involves modifying the gene expression of an organism, while sensitivity analysis examines the response of a system to changes in its inputs.

Genetic algorithm is a stochastic global search optimization method that has limitations in local search. SA well characterizes the impact of parameter variations on the output of the algorithm model and is beneficial for improving the local search capability of genetic algorithm.

The selection operation employs both the elitist preservation and roulette wheel strategies to ensure the accuracy of optimization results. The crossover operation utilizes the two-parent single-point crossover strategy to reasonably control the crossover point to ensure sufficient gene exchange. The mutation operation adopts a random bitwise flip strategy, where only one bit is changed per mutation event.

Fig. 4 shows the flowchart of sensitivity analyses at the end of each genetic iteration, and only two parameters are shown to make it more intuitive. First, the binary sequences are transformed into decimal number. Then, add or subtract the step size to each parameter to obtain combinations of three numbers. Finally, calculate the fitness value of each combination to find the max fitness value and ascertain the direction of sensitivity vectors (SV).
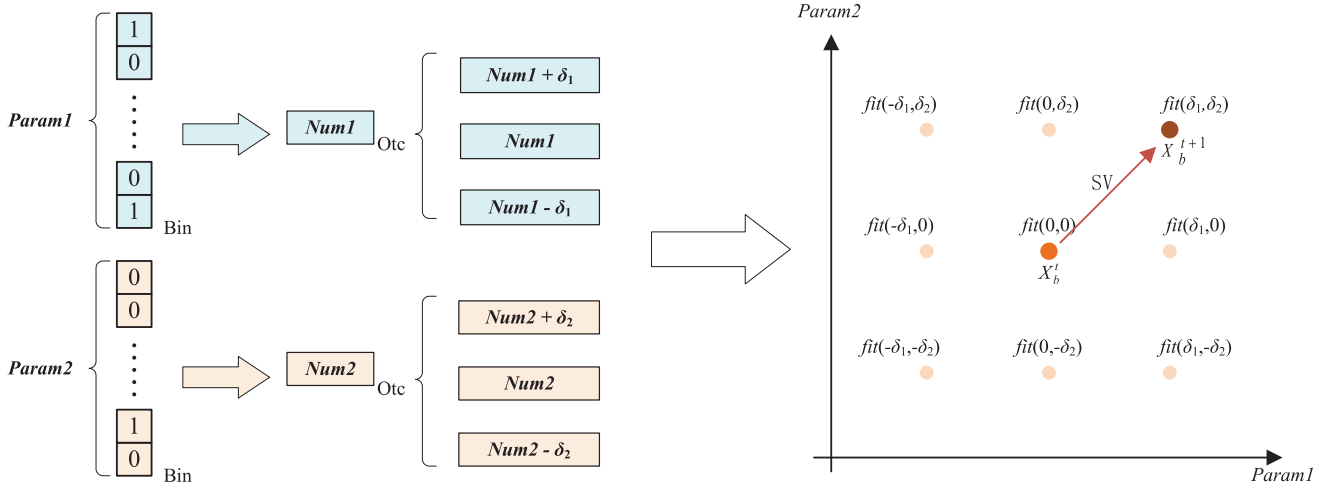

Figure 4. Flow chart of SA.

For the optimal structure parameter search problem of 1D D-EBG, sensitivity vectors of the objective function with each design parameter are obtained. The direction with the maximum sensitivity vector is selected as the search direction. It can be expressed as

$$\nabla f(X_b) = \left(\frac{\partial f}{\partial x_1}, \frac{\partial f}{\partial x_2}, \dots, \frac{\partial f}{\partial x_m} \right) \tag{29}$$

Let X_b be the individual with the maximum fitness in the population and $f(X)$ be a non-differentiable function of m dimensions. The next generation's parameter can be represented as

$$x_i^{t+1} = \begin{cases} x_i^t + \delta_i \cdot \nabla f(x_i), f(x_i + \Delta x_i) > f(x_i) \\ x_i^t - \delta_i \cdot \nabla f(x_i), f(x_i + \Delta x_i) < f(x_i) \end{cases} \tag{30}$$

The symbol δ_i denotes the iterative step size, which is set to a relatively small positive number determined by the design accuracy of the i-th parameter. The variable t represents the current iteration index. If the sensitivity vector points towards the direction in which the objective function increases, moving the parameter x_i towards this direction results in obtaining the maximum value. Conversely, moving in the opposite direction will yield the minimum value.

Performing SA on the best individual in the population and computing its fitness function allows replacing the individual with the lowest fitness value with the newly generated offspring as a part of the iteration process. This ensures that the newly generated individuals are more likely to have better fitness values, promoting the convergence of the optimization algorithm.

3.2.3. Stage 3: Reconstruction of the Fitness Function

Although the sensitivity analysis in stage 2 already enabled us to obtain a parameter combination with the highest relative fitness, it is necessary to dynamically adjust the results for better engineering

application, considering the actual accuracy of the materials used and the dimensional errors introduced during processing.

To this end, a new fitness function has been constructed based on an improved version of (28). This fitness function replaces the original fitness value of a parameter at x with the average fitness value over its neighborhood $(x - \triangle x, x + \triangle x)$.

Since the original fitness function $f(x)$ is discrete, it must be first fitted into a smooth continuous curve using a cubic spline interpolation method for the purpose of function integration. Cubic spline interpolation is a widely-used method for fitting curves between discrete data points [27]. It employs cubic polynomials to approximate the curves between data points of each adjacent pair, and enforces smoothness and accuracy of the resulting interpolant by satisfying several conditions. Compared to other interpolation methods, cubic spline interpolation can avoid oscillations and overshoots, making it more reliable and accurate in practical applications.

As shown in (31), the new fitness function, denoted as $newf(x)$, is defined as the average fitness of a parameter at x with its neighborhood $(x - \triangle x, x + \triangle x)$.

$$newf(x) = \frac{1}{2 \times \triangle x} \int_{x-\triangle x}^{x+\triangle x} S(x)dx \qquad (31)$$

To begin, we will employ the cubic spline interpolation method to convert the discrete data points into a continuous curve. Next, we will utilize the enhanced fitness function outlined by (31).

$$y = \begin{cases} 0, & 0 \le x < 0.9 \\ 1/x, & 0.9 \le x < 1.6 \\ 0, & 1.6 \le x \le 2.2 \end{cases} \qquad (32)$$

Figure 5 illustrates the cubic spline interpolation of data points and new fitness curve generated by MATLAB. The original discrete points were generated at intervals of 0.1 using (32). The interpolation curve is generated based on the original fitness discrete points using a cubic spline interpolation method.

The new fitness curve is a great improvement over the interpolated curve. Firstly, the new fitness function eliminates discontinuities, making the curve smoother and better reflecting the average
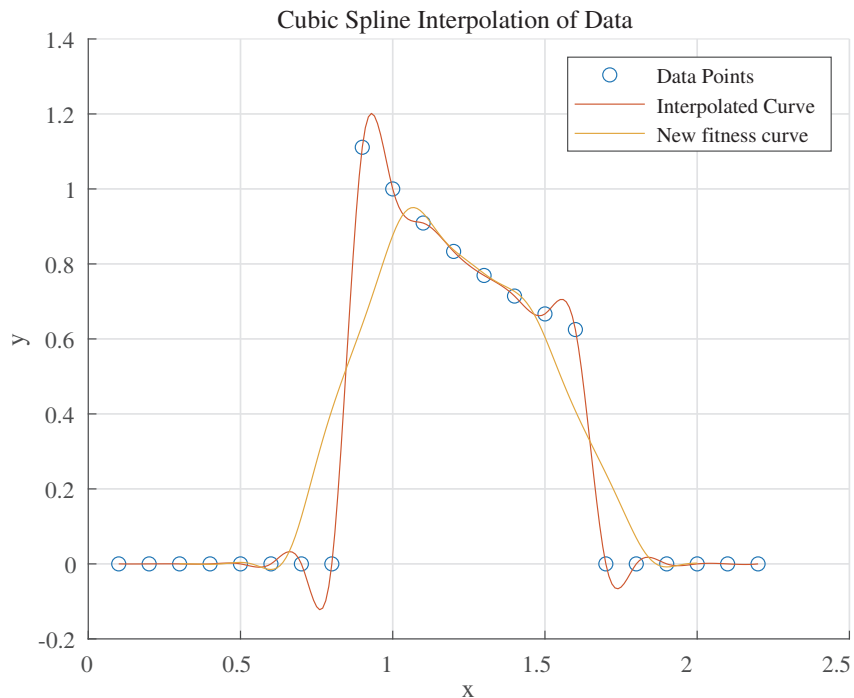

Figure 5. Cubic spline interpolation of data and new fitness curve.

fitness level as parameters vary within a region. Secondly, the new fitness function fully utilizes the complex coupling relationships between parameters, providing a more realistic description of the relationship between EBG design parameters and the stopband performance target. Thirdly, while ensuring computational accuracy, the new function enhances algorithm stability by effectively reducing oscillations in the optimization target caused by parameter deviations, better meeting the robustness requirements of engineering design optimization.

4. RESULT ANALYSIS

To validate the feasibility of the proposed MS-GA in optimal parameter search for any stopband, multiple schemes were designed for different design options and optimization parameters. The simulation results were verified using three-dimensional full wave simulation software Ansoft HFSS.

4.1. Dual-Parameter Optimization with Fixed width of HK

Considering the dual-parameter optimization of dielectric constant (ε_r) and periodicity length (p) for high dielectric constant ceramics with fixed width (w_c), we aim to investigate the impact of parameter changes on bandgap while meeting the requirements of small size and material characteristics.

4.1.1. Design Objectives and Iterative Process

To achieve this goal, we restrict the optimized parameters by fixing the width of the high dielectric unit (w_c) at 0.5 mm, setting the maximum dielectric constant (ε_r) to 2000, and the periodicity length (p) is from 1 mm to 4 mm.

Aim parameters and final results of two design schemes are presented in Table 1. Consider a genetic algorithm for optimizing the parameter of dielectric constant ε_r, where the gene length for is 6 with a minimum change of 31.73 ($(2000 - 1)/(2^6 - 1) = 31.73$), and the gene length for p is 6 with a minimum change of 0.048 mm ($(4 - 1)/(2^6 - 1) = 0.048$). The minimum Hamming distance D between two individuals is 7 ($(6 + 6)/2 + 1 = 7$).

Table 1. Dual-parameter optimization.

Scheme No.	Aim		Preliminary Result			Final Result		
	f_{set}/GHz	S_{set}/dB	ε_{r}	p/mm	N_{p}	ε_{r}	p/mm	N_{p}
1	$3.4 \sim 3.6$	-80	1469	4	4	1565	4	4
2	$26.5 \sim 29.5$	-100	790	2.3	5	726	2.3	5

Table 2 presents the impact of the number of periods (N_{p}) and the initial population size (N) on the number of individuals with a non-zero fitness. It should be noted that each generation is initialized with random individuals, and the final result is obtained by averaging the number of successful individuals over five trials.

Table 2. Effect of the period number (N_{p}) and population size (N) on the number of non-zero fitness individuals for Scheme 1/Scheme 2.

N_{p} \ N	30	40	50	60	70
3	0/0	0/0	0/0	0/0	0/0
4	3/0	4.6/0	4.4/0	6/0	4.8/0
5	6.6/4.2	11/6.6	13.4/6.2	14/6.4	19.4/6.5
6	*/6.6	*/9	*/10.6	*/13.4	*/15.2

The analysis reveals that at $N_{\mathrm{p}} = 3$, no individuals with fitness greater than 0 appear in any population size. However, at $N_{\mathrm{p}} = 4$ for scheme 1 and $N_{\mathrm{p}} = 5$ for scheme 2, a population initialized using Hamming distance population (HD pop) has individuals with fitness greater than 0, which comprise approximately 10% of the population. Therefore, to achieve miniaturization of EBG structure, it can be determined that a population size of $N = 50$, $N_{\mathrm{p}} = 4$ for scheme 1 and $N_{\mathrm{p}} = 5$ for scheme 2 is appropriate. Fig. 6 depicts the fitness levels of each individual in a Hamming distance initialized population during a single fitness test.
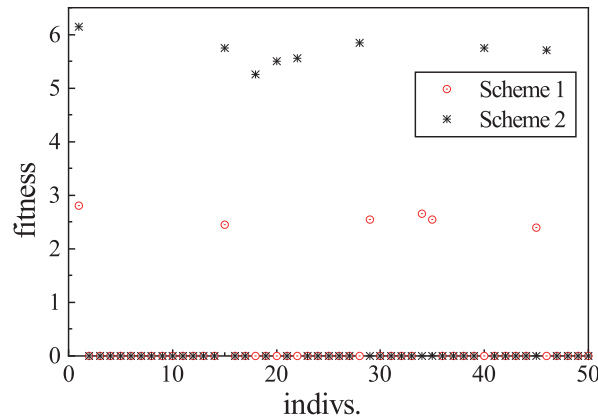

Figure 6. Fitness of hamming initialized population ($w_c = 0.5\,\mathrm{mm}$, $N_{\mathrm{p}} = 4$ for Scheme 1, $N_{\mathrm{p}} = 5$ for Scheme 2).

A genetic algorithm combined with sensitivity analysis will be utilized to ensure that a better local solution is obtained before each iteration ends. Fig. 7 compares the convergence effects of each iteration before and after incorporating sensitivity analysis for each design scheme. The traditional random search-based genetic algorithm gradually increased the fitness from 2.8 to 2.95 over 10 iterations due to its undirected search. However, there was little or no difference between the results of each iteration, and the optimal solution was not found within 10 iterations. After incorporating sensitivity analysis, the fitness gradually increased from 2.8 to 3.25 over 5 iterations for scheme 1. The algorithm always moved in the direction of higher fitness, thus finding a better solution than the previous iteration before each iteration ended.
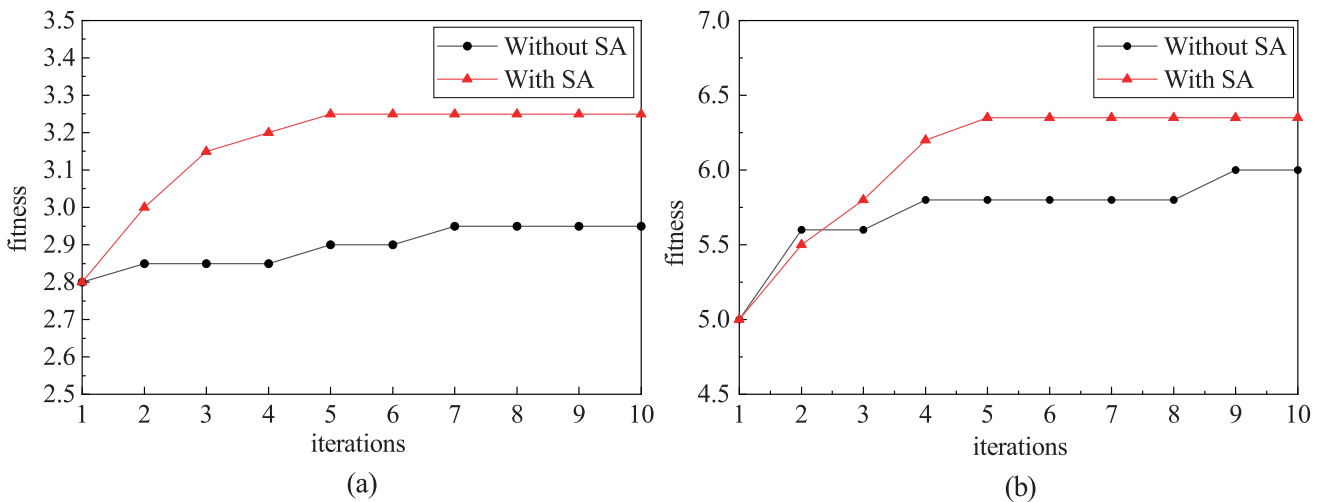

Figure 7. Compare of trace with SA and without SA. (a) Scheme 1. (b) Scheme 2.

4.1.2. Adjustment of Result

In the previous stage of our investigation, we utilized genetic operations in combination with sensitivity analysis to identify the individual with optimal fitness. For scheme 1, the aim was to achieve $f_{\text{set}} = (3.4\,\text{GHz},\ 3.6\,\text{GHz})$ and $S_{\text{set}} = -80\,\text{dB}$, resulting in $\varepsilon_r = 1469$, $p = 4\,\text{mm}$, and $N_{\text{p}} = 4$. For scheme 2, the aim was to obtain $f_{\text{set}} = (26.5\,\text{GHz},\ 29.5\,\text{GHz})$ and $S_{\text{set}} = -100\,\text{dB}$, resulting in $\varepsilon_r = 790$, $p = 2.3\,\text{mm}$, and $N_{\text{p}} = 5$.

In this phase of our investigation, we conducted a parameter scan in the vicinity of the obtained results and acquired discrete points for the original fitness function. We then applied two-dimensional cubic spline interpolation to fit the data. Specifically, we performed a scan for the dielectric constant ε_r within the range of $(\varepsilon_r - \triangle\varepsilon_r,\ \varepsilon_r + \triangle\varepsilon_r)$ and for the period p within the range of $(p - \triangle p,\ p + \triangle p)$. In this study, we chose $\triangle\varepsilon_r = 100$ and $\triangle p = 0.2\,\text{mm}$ as the parameter intervals.

Figure 8 displays the three-dimensional plots of fitness as a function of dielectric constant and period length, both for the fitted data using a two-dimensional cubic spline interpolation and for the fitness function improved through modifications. Figs. 8(a) and (b) reveal a steep slope at the boundary between zero and non-zero fitness for the interpolated data, whereas the modified fitness function exhibits a more gradual relative change and peaks at $\varepsilon_r = 1343$ and $p = 4.6\,\text{mm}$. However, considering the maximum allowable period length of $4\,\text{mm}$ in this approach, the optimal solution is adjusted to $\varepsilon_r = 1565$ and $p = 4\,\text{mm}$. Similarly, Figs. 8(d) and (e) depict the three-dimensional relationship visualization results for scheme 2, indicating that the optimal fitness is achieved at $\varepsilon_r = 726$ and $p = 2.3\,\text{mm}$.
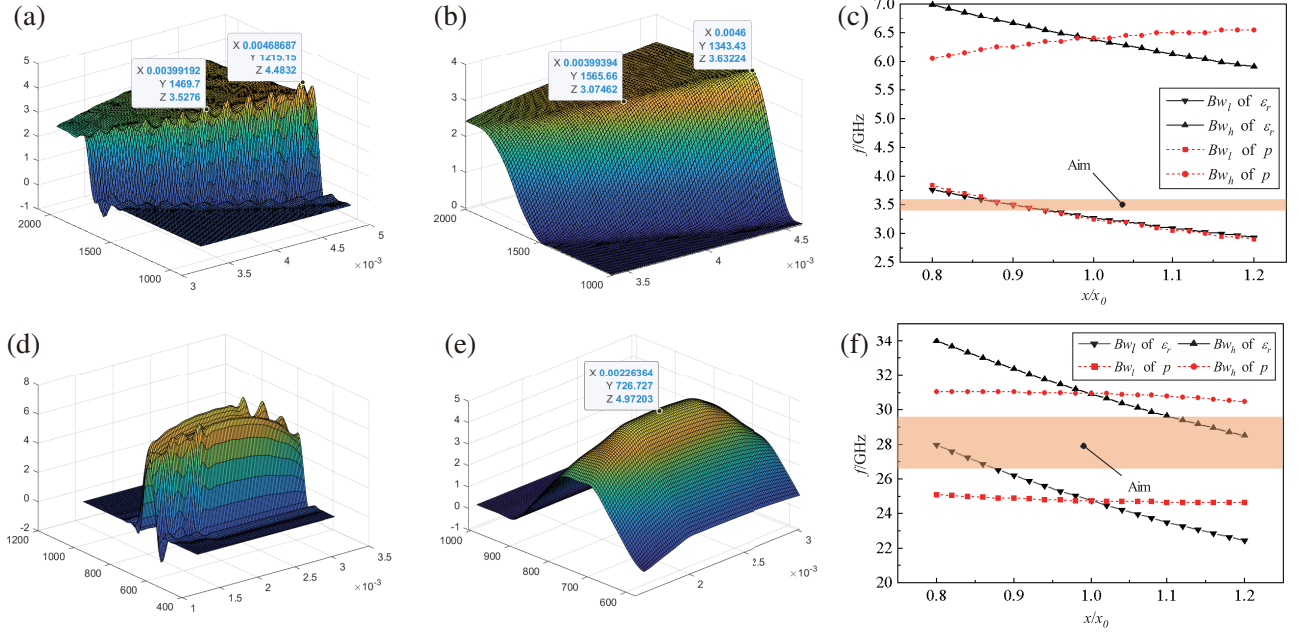

Figure 8. Results of two schemes.(p is in meters) (a) Cubic spline interpolation of $f(x)$ for Scheme 1. (b) Using $newf(x)$ for Scheme 1. (c) The influence of each parameter on stopband for Scheme 1. (d)Cubic spline interpolation of $f(x)$ for Scheme 2. (e) Using $newf(x)$ for Scheme 2. (f) The influence of each parameter on stopband for scheme 2. (Another parameter is fixed).

To better understand the effect of parameter variations on the stopband of the two proposed designs, a detailed analysis was conducted on the results of both schemes. Figs. 8(c) and (f) illustrate the impact of changes in the design parameters ε_r and p on the stopband range. Here, x/x_0 represents the ratio of the calculated parameters to the optimal parameters, which was constrained to fall within the range of 0.8 to 1.2 in order to accurately reflect their influence on the stopband.

As shown in Fig. 8(c), for scheme 1, at the optimal result ($x/x_0 = 1$), the center frequency of the

stopband was 4.7 GHz with a bandwidth of 3 GHz. As the dielectric constant increased, the center of the stopband shifted downwards while the bandwidth slightly decreased. However, as the periodic length increased, the center of the stopband moved slightly downward while the bandwidth gradually increased. Similarly, for scheme 2, as depicted in Fig. 8(f), at the optimal result ($x/x_0 = 1$), the center frequency of the stopband was 28.1 GHz with a bandwidth of 6.1 GHz. With an increase in the dielectric constant, the center of the stopband shifted downward while the bandwidth remained relatively unchanged. At the optimal result, the stopband reached its widest point as the periodic length increased, but the bandwidth on either side of the center frequency slightly narrowed.

4.2. Full-Parameter Optimization

4.2.1. Design Objectives and Iterative Process

The filling ratio of high dielectric constant units in a period has a significant impact on the bandgap width [28]. Incorporating the filling of high dielectric constant materials into the optimization of 1D D-EBG can further widen the bandgap and achieve higher noise isolation. To ensure that the final results satisfy both size and material requirements, we set the maximum value of the dielectric constant (ε_r) at 2000, the period length (p) between 1 mm and 4 mm, and the filling ratio (r) of high dielectric constant units between 1% and 50%.

Table 3 illustrates the specific optimization objectives and results for scheme 3, while Table 4 lists the parameter changes in each iteration. As can be seen from the results, for scheme 3, the optimized values of ε_r and p both reached their maximum values after the 9th iteration, which are 2000 and 4 mm, respectively. The obtained filling ratio of high dielectric constant units was 12.9%, which is relatively small.

Table 3. Full-parameter optimization.

Scheme No.	Aim		Preliminary Result				Final Result			
	f_{set}/GHz	S_{set}/dB	ε_r	p/mm	r	N_{p}	ε_r	p/mm	r	N_{p}
3	2.2~2.6	−80	2000	4	12.3%	5	2000	4	12.9%	5

Table 4. Results of full parameter iteration.

iteration	ε_r	p	r	fitness
1	1611	3.94	17.1%	2.90
2	1660	4.00	16.3%	3.10
3	1709	4.00	16.3%	3.15
4	1758	4.00	15.6%	3.35
5	1807	3.90	15.1%	3.40
6	1855	4.00	14.4%	3.65
7	1904	3.89	14.4%	3.70
8	2000	3.94	13.9%	4..05
9	2000	4.00	12.3%	4.20
10	2000	4.00	12.3%	4.20

4.2.2. Adjustment and Correlation of Each Parameter

Figures 9(a) and (b) depict the relationship between the continuousization of the discrete points of the original fitness value using cubic spline interpolation and the subsequent averaging process in three
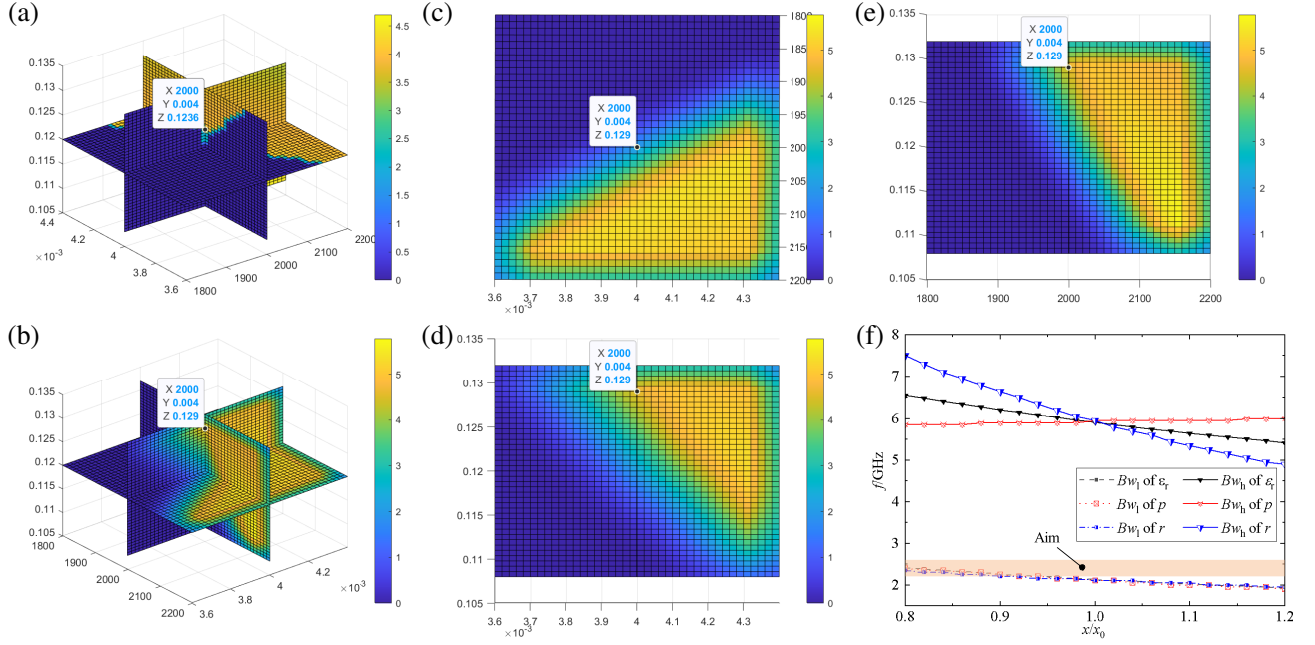
Figure 9. (a) Results of cubic spline linear interpolation using $f(x)$ for Scheme 3. (b) Results using $newf(x)$ for Scheme 3. (c) The influence of ε_r and p on fitness. (d) The influence of r and p on fitness. (e) The influence of ε_r and r on fitness. (f) The influence of each parameter on stopband. (the other parameters are fixed).

Table 5. Correlation coefficient of each parameter.

	ε_r	p	r	Bw(fitness)
ε_r	1	-0.345	-0.117	-0.011
p	-0.345	1	-0.269	-0.116
r	-0.117	-0.269	1	-0.882
Bw(fitness)	-0.011	-0.116	-0.882	1

directions based on a new fitness function. The parameter ranges for parameter variations are set as follows: $\Delta\varepsilon_r = 100$, $\Delta p = 0.2\,\mathrm{mm}$, $\Delta r = 0.6\%$.

It can be observed that the local mean calculation results in a smoother outcome compared to the interpolation results. The final adjusted values are ($\varepsilon_r = 2000$, $p = 4\,\mathrm{mm}$, $r = 12.9\%$). Figs. 9(c) to (e) illustrate the impact patterns between each pair of design parameters on fitness.

Figure 9(f) presents the influence of individual parameters on the stopband range. It can be observed that the proposed structure achieves a bandwidth of $3.8\,\mathrm{GHz}$ within the frequency range of $2.1\,\mathrm{GHz}$ to $5.9\,\mathrm{GHz}$, with a noise suppression depth of $80\,\mathrm{dB}$ in the stopband. As the parameters gradually increase from $0.8x_0$ to $1.2x_0$, where x_0 is the optimal result of each parameter, the bandwidth narrows down and shifts towards lower frequencies.

To investigate the impact of various parameters on the stopband of the one-dimensional dielectric bandgap structure and the correlation among constitutive parameters (such as relative permittivity, ε_r, period length, p, and filling ratio, r), a parameter scan was conducted around the results obtained by a multi-stage genetic algorithm ($\varepsilon_r = 2000$, $p = 4\,\mathrm{mm}$, $r = 12.3\%$). Multiple sets of parameters were used to explore the stopband characteristics. The employed database contains optimized design parameters and corresponding bandwidths of 1D D-EBG that contain the target frequency range. A four-dimensional visualization plot was generated using MATLAB to illustrate the interplay of these
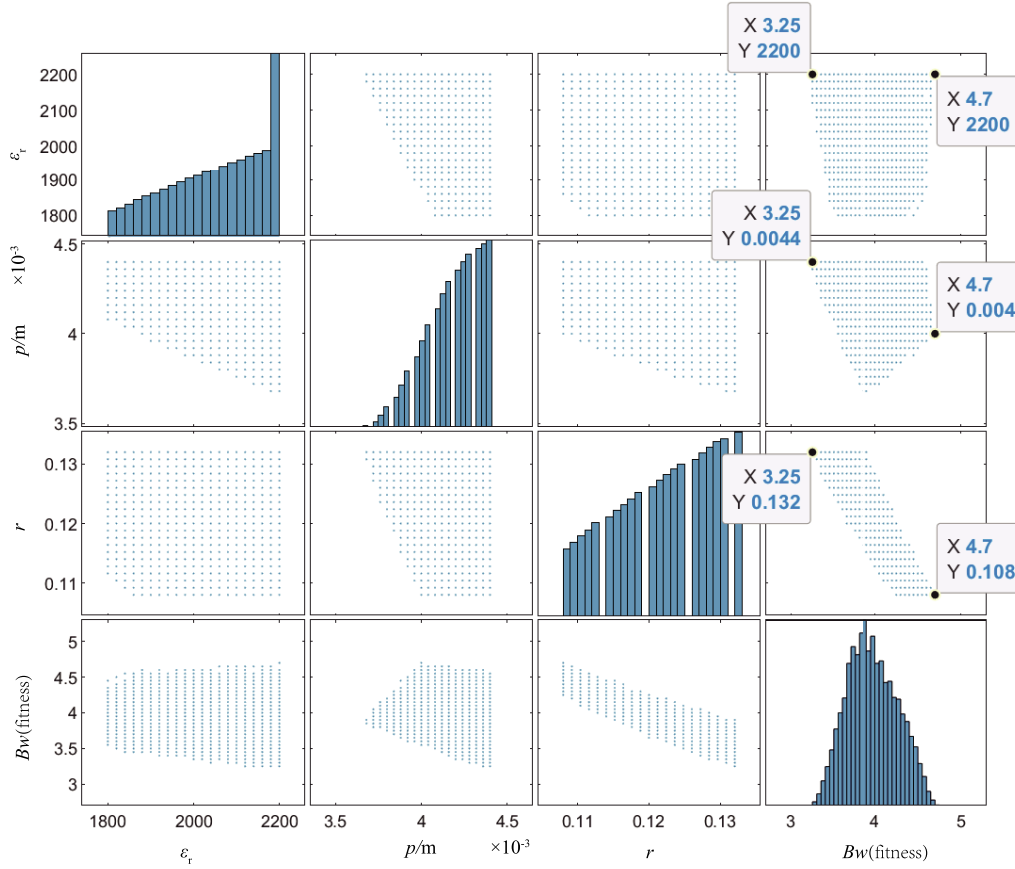
Figure 10. Influence of each parameter on fitness and their relevance.

parameters, as depicted in Fig. 10.

The main diagonal subplots (top-left to bottom-right) represent histograms displaying the distribution of each variable. The off-diagonal subplots are scatter plots illustrating the relationships between two variables.

Table 5 presents the Pearson correlation coefficients between the various parameters and stopband bandwidths. These coefficients, ranging from -1 to 1, quantify the degree of correlation. The Pearson correlation coefficient can be calculated using

$$R = Cov(X, Y)/(std(X) * std(Y)) \tag{33}$$

where $Cov(X, Y)$ represents the covariance between variables X and Y, and $std(X)$ and $std(Y)$ represent the standard deviations of X and Y, respectively. By calculating the covariance and standard deviations of two variables, we can obtain their correlation coefficient, which allows us to assess the strength of their relationship.

The correlation coefficient between ε_r and Bw is -0.011, indicating a nearly negligible linear relationship between them. When the dielectric constant varies over a large range, it is still possible to achieve a stopband containing the specified target by adjusting the other two parameters. The correlation coefficient between p and Bw is -0.116, suggesting a weak negative correlation between them. From Fig. 10, it can be observed that when the period length is $4\,\mathrm{mm}$, the widest stopband can be achieved by adjusting the remaining two parameters, gradually narrowing the bandwidth as the period length extends. The correlation coefficient between ε_r and p is -0.345, which implies a moderate negative correlation between them. The correlation coefficient between ε_r and r is -0.117, indicating a weak negative correlation between them. The correlation coefficient between p and r is -0.269, which suggests a certain degree of negative correlation between them. As p increases, r tends to decrease.

4.3. Stimulation of Result

To verify whether the optimized results meet the required isolation performance, a full-wave simulation software was used to simulate and validate the optimal parameters of the designed scheme 1D D-EBG model as shown in Figs. 11(a) and (b). The simulation model was established based on a multi-layer PCB consisting of a pair of power/ground planes, with copper foil covering both the top and bottom surfaces of the substrate. The substrate was made of Rogers RT/duroid 5880 material ($\varepsilon_{r2} = 2.2$), and 4 high dielectric constant ceramic materials with $\varepsilon_{r1} = 1565$ were periodically embedded in the substrate, with a width of $w_c = 0.5\,\text{mm}$ and an EBG period length of $p = 4\,\text{mm}$. The total length of the PCB was $l = 20\,\text{mm}$, the width $w = 5\,\text{mm}$, and the thickness $h = 0.2\,\text{mm}$.
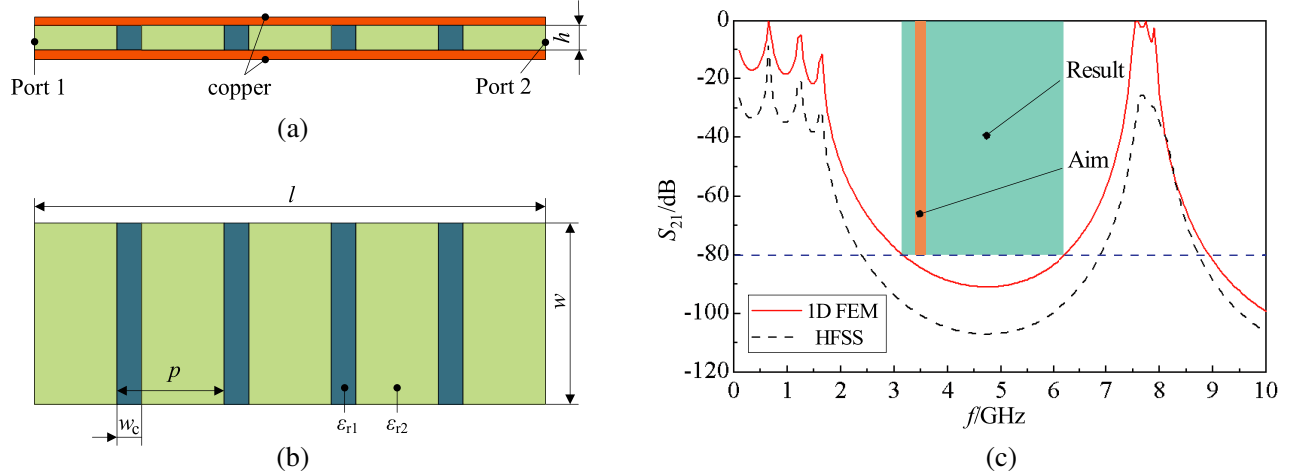

Figure 11. Modeling and verify for 1D D-EBG. (a) Front view (with copper clad surface). (b) Top view (without copper clad surface). (c) Comparison of 1D-FEM calculation and simulation results

As shown in Fig. 11(c), taking $S_{\text{set}} = -80\,\text{dB}$ and using MS-GA, the optimized bandgap $B_{\text{gap}} = (3.2\,\text{GHz}, 6.2\,\text{GHz})$ with a bandwidth of $Bw = 3\,\text{GHz}$ was obtained, which encompasses the target frequency range $f_{\text{set}} = (3.4\,\text{GHz},\ 3.6\,\text{GHz})$ and meets the design requirements. Additionally, there was significant suppression of out-of-band noise. This scheme utilized 4 periods, and the total length of the 1D D-EBG structure is 16 mm, making it suitable for noise isolation in small-sized devices.

There is a significant difference in noise isolation between the 1D finite element method (FEM) and 3D simulation models within the stopband. The noise isolation of the 1D FEM model is greater than 80 dB in the target frequency band, while the HFSS result is greater than 100 dB, and the obtained stopband from HFSS is also wider than the 1D FEM. The main reasons for these differences are: Firstly, the 1D FEM model assumes that excitation fields propagate in a single plane only, while 3D simulation considers field distribution in multiple dimensions. In the 3D case, the proportion of excitation fields along the electromagnetic wave transmission direction decreases, thereby greatly reducing the coupled field strength at the receiving end and exhibiting higher noise isolation. Secondly, after embedding high dielectric constant materials in the dielectric substrate, the structural capacitance is enhanced. For the 1D model, capacitance only reflects the capacitive characteristics of the structure in a single dimension, while the 3D model considers the combined capacitive properties in three directions. The increase of structural capacitance in the 3D model can further reduce cross-coupling in multiple dimensions, thereby improving noise isolation capability.

In summary, the differences in calculation results are mainly due to multi-directional coupling effects and structural capacitance, which does not undermine the accuracy of 1D FEM in predicting the stopband location of the 1D D-EBG structure with limited periods.

5. CONCLUSION

In this work, we successfully applied a multistage genetic algorithm (MS-GA) optimization method considering parameter variations to optimize one-dimensional dielectric bandgap (D-EBG) structures with a few periods in small packaging power distribution networks. One-dimensional finite element method (1D FEM) was used to find the stopband with specified isolation. In stage 1, a hamming distance initialization population is used to detect the existence of the bandgap by specifying an isolation degree to define the bandgap, thereby avoiding infinite periodic dispersion calculations. In stage 2, sensitivity analysis is applied in each genetic iteration to improve the algorithm's local search ability. In stage 3, the optimization results are adjusted using a new fitness function generated by cubic spline interpolation and integral function based on parameter variations. The resulting outcomes conform to the optimization criteria within the acceptable range of parameter errors and enhance the robustness of the designed structure. In addition, the variations of the stopband relative to different design parameters and assessing their correlations are analyzed, and all three proposed designs have final dimensions below 20 mm. The automated design method presented in this study holds great promise for optimizing the design parameters of multidimensional EBGs in multilayer small packaging substrates, enabling wide bandgaps and high noise isolation. Future research directions could explore additional dimensions and further experimentally validate the proposed methodology.

ACKNOWLEDGMENT

REFERENCES

1. Guang, T. L., R. W. Techentin, and B. K. Gilbert, "High-frequency characterization of power/ground-plane structures," *IEEE Trans. Microw. Theory Tech.*, Vol. 47, No. 5, 562–569, May 1999.

2. Cui, W., J. Fan, Y. Ren, H. Shi, J. L. Drewniak, and R. E. DuBroff, "DC power-bus noise isolation with power-plane segmentation," *IEEE Trans. Electromagn. Compat.*, Vol. 45, No. 2, 436–443, May 2003.

3. Xu, M., T. H. Hubing, J. Chen, T. P. van Doren, J. L. Drewniak, and R. E. DuBroff, "Power-bus decoupling with embedded capacitance in printed circuit board design," *IEEE Trans. Electromagn. Compat.* Vol. 45, No. 1, 22–30, Feb. 2003.

4. Sievenpiper, D., L. Zhang, R. F. J. Broas, N. G. Alexopolous, and E. Yablonovitch, "DC power-bus noise isolation with power-plane segmentation," *IEEE Trans. Microw. Theory Tech.*, Vol. 47, No. 11, 2059–2074, Nov. 1999.

5. Yang, F. R., K. P. Ma, Y. Qian, and T. Itoh, "A novel TEM-waveguide using uniplanar compact photonic band-gap (UC-PBG) structure," *APMC 1999*, Vol. 2, Cat. No. 99TH8473, 323–326, 1999.

6. Chappell, W. J. and X. Gong, "Wide bandgap composite EBG substrates," *IEEE Trans. Antennas Propag.*, Vol. 51, No. 10, 2744–2750, Oct. 2003.

7. Pani, P. R., R. K. Nagpal, R. Malik, N. Gupta, et al., "Design of planar EBG structures using cuckoo search algorithm for power/ground noise suppression," *Progress In Electromagnetics Research M*, Vol. 28, 145–155, 2013.

8. Kim, T. H., M. Swaminathan, A. E. Engin, and B. J. Yang, "Electromagnetic band gap synthesis using genetic algorithms for mixed signal applications," *IEEE Trans. Adv. Packag.*, Vol. 32, No. 1, 13–25, Feb. 2009.

9. Kovacs, P., Z. Raida, Techentin, and B. K. Gilbert, "Global evolutionary algorithms in the design of electromagnetic band gap structures with suppressed surface waves propagation," *Radioeng.*, Vol. 19, No. 1, 122–128, 2010.

10. Tripathi, J. N., N. K. Chhabra, R. K. Nagpal, R. Malik, and J. Mukherjee, "Damping the cavity-mode anti-resonances' peaks on a power plane by swarm intelligence algorithms," *ISCAS 2012*, 361–364, 2012.

11. Haupt, R. L., "An introduction to genetic algorithms for electromagnetics," *IEEE Antennas Propag. Mag.*, Vol. 37, No. 2, 7–15, Apr. 1995.

12. Vasconcelos, J. A., R. Saldanha, L. Krahenbuhl, and A. Nicolas, "Genetic algorithm coupled with a deterministic method for optimization in electro-magnetics," *IEEE Trans. Magn.*, Vol. 33, No. 2, 1860–1863, Mar. 1997.

13. Villegas, F., T. Cwik, Y. Rahmat-Samii, and M. Manteghi, "A parallel electromagnetic genetic-algorithm optimization (EGO) application for patch antenna design," *IEEE Trans. Antennas Propag.*, Vol. 52, No. 9, 2424–2435, Sep. 2004.

14. Caorsi, S., A. Costa, and M. Pastorino, "Microwave imaging within the second-order Born approximation: Stochastic optimization by a genetic algorithm," *IEEE Trans. Antennas Propag.*, Vol. 49, No. 1, 22–31, Jan. 2001.

15. Venkatarayalu, N., T. Ray, and Y.-B. Gan, "Multilayer dielectric filter design using a multiobjective evolutionary algorithm," *IEEE Trans. Antennas Propag.*, Vol. 53, No. 11, 3625–3632, Nov. 2005

16. Karatzidis, D. I., N. V. Kantartzis, G. G. Pyrialakos, T. V. Yioultsis, and C. S. Antonopoulos, "Genetic optimization with mixed-order prism macroelements for 3-D metamaterial multilayered structures," *IEEE Trans. Magn.*, Vol. 55, No. 6, 1–4, Jun. 2019.

17. Choi, K., D.-H. Jang, S.-I. Kang, J.-H. Lee, T.-K. Chung, and H.-S. Kim, "Hybrid algorithm combing genetic algorithm with evolution strategy for antenna design," *IEEE Trans. Magn.*, Vol. 52, No. 3, 1–4, Mar. 2016.

18. Xiao, F., D. Yan, and L. Sun, "Optimization design of ground plane PBG structure of T-shape microstrip line by improved FGA," *ICMMT*, Vol. 3, 1561–1564, Apr. 2008.

19. Zhu, H.-R., J.-B. Wang, Y.-F. Sun, and X.-L. Wu, "An improved genetic algorithm for optimizing EBG structure with ultra-wideband SSN suppression performance of mixed signal systems," *IEEE Access*, Vol. 8, 26129–26138, 2020.

20. Zhu, H.-R., J.-B. Wang, Y.-F. Sun, X.-L. Wu, and J.-F. Mao, "A novel automatically designed EBG structure by improved GA for ultrawideband SSN mitigation of system in package," *Packag. Manuf. Technol.*, Vol. 10, No. 1, 123–133, Jan. 2020.

21. Vieira, D. G., D. A. G. Vieira, W. M. Caminhas, and J. A. Vasconcelos, "Hybrid approach combining genetic algorithm and sensitivity information extracted from a parallel layer perceptron," *IEEE Trans. Magn.*, Vol. 41, No. 5, 1740–1743, May 2005.

22. Lin, B.-Q., Q.-R. Zheng, and N.-C. Yuan, "A novel planar PBG structure for size reduction," *IEEE Microw. Wirel. Compon. Lett.*, Vol. 16, No. 5, 269–271, May 2006.

23. Barth, S. and A. K. Iyer, "The MTM-EBG as a rigorous multiconductor model of the UC-EBG and approaches for miniaturization," *IEEE Trans. Antennas Propag.*, Vol. 70, No. 4, 2822–2831, Apr. 2022.

24. Wang, W., X.-Y. Cao, W.-Y. Zhou, and L. Tao, "A novel compact uni-planar electromagnetic band-gap (UC-EBG) structure," *ICMMT*, Vol. 4, No. 4, 1634–1636, Apr. 2008.

25. Toyota, Y., A. E. Engin, T. H. Kim, M. Swaminathan, and S. Bhattacharya, "Size reduction of electromagnetic bandgap (EBG) structures with new geometries and materials," *ECTC*, Jun. 2006.

26. Jin, J. M., *The Finite Element Method in Electromagnetics*, John Wiley and Sons, New York, 2015.

27. McKinley, S. and M. Levine, "Cubic spline interpolation," *College of the Redwoods*, Vol. 45, No. 1, 1049–1060, 1998.

28. Shi, P., K. Huang, and Y. Li, "Photonic crystal with complex unit cell for large complete band gap," *Opt. Commun.*, Vol. 285, No. 13–14, 3128–3132, 2012.